AD-A147 006 THERMAL EVAPORATION IN BLAST WAVES: A MODEL FOR ANEURISM FORMATION IN THE..(U) NAVAL RESEARCH LAB WASHINGTON DC J L GIULIANI 11 OCT 84 NRL-MR-5420 1/1

UNCLASSIFIED F/G 19/4 NL

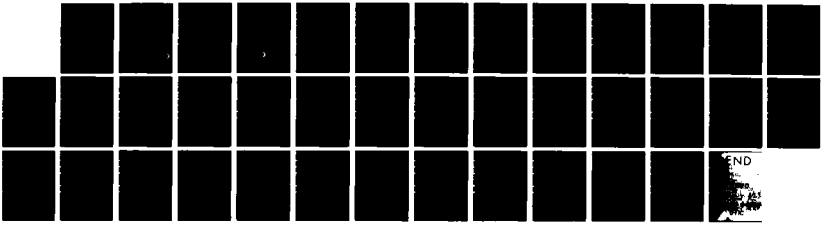

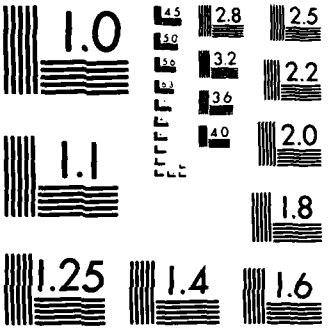

(2)

NRL Memorandum Report 5420

Thermal Evaporation in Blast Waves: A Model for Aneurism Formation in the NRL LASER-HANE Simulation Experiment

J. L. GIULIANI, JR.

Geophysical and Plasma Dynamics Branch
Plasma Physics Division

October 11, 1984

This research was partially sponsored by the Defense Nuclear Agency under Subtask S99QMXBC, work unit 00102 and work unit title "Plasma Structure Evolution."

NAVAL RESEARCH LABORATORY
Washington, D.C.

Approved for public release; distribution unlimited.

SECURITY CLASSIFICATION OF THIS PAGE

REPORT DOCUMENTATION PAGE

1a REPORT SECURITY CLASSIFICATION UNCLASSIFIED	1b RESTRICTIVE MARKINGS
2a SECURITY CLASSIFICATION AUTHORITY	3 DISTRIBUTION/AVAILABILITY OF REPORT Approved for public release; distribution unlimited.
2b DECLASSIFICATION/DOWNGRADING SCHEDULE	
4 PERFORMING ORGANIZATION REPORT NUMBER(S) NRL Memorandum Report 5420	5 MONITORING ORGANIZATION REPORT NUMBER(S)
6a NAME OF PERFORMING ORGANIZATION Naval Research Laboratory	6b OFFICE SYMBOL (If applicable) Code 4780
6c ADDRESS (City, State, and ZIP Code) Washington, DC 20375-5000	7a NAME OF MONITORING ORGANIZATION 7b ADDRESS (City, State, and ZIP Code)
8a NAME OF FUNDING/SPONSORING ORGANIZATION Defense Nuclear Agency	8b OFFICE SYMBOL (If applicable) RAAE
8c ADDRESS (City, State, and ZIP Code) Washington, DC 20305	9 PROCUREMENT INSTRUMENT IDENTIFICATION NUMBER 10 SOURCE OF FUNDING NUMBERS

PROGRAM ELEMENT NO	PROJECT NO	TASK NO	WORK UNIT ACCESSION NO
62715H			DN580-072

11 TITLE (Include Security Classification)
Thermal Evaporation in Blast Waves: A Model for Aneurism Formation in the NRL LASER-HANE Simulation Experiment

12 PERSONAL AUTHOR(S)
Giuliani, J.L., Jr.

13a TYPE OF REPORT	13b TIME COVERED	14 DATE OF REPORT (Year, Month, Day)	15 PAGE COUNT
Interim	FROM 10/83 TO 10/84	1984 October 11	39

16 SUPPLEMENTARY NOTATION This research was partially sponsored by the Defense Nuclear Agency under Subtask S99QMXBC, work unit 00102 and work unit title "Plasma Structure Evolution."

17 COSATI CODES		
FIELD	GROUP	SUB-GROUP

18 SUBJECT TERMS (Continue on reverse if necessary and identify by block number)
Blast wave — Magnetic fields
Laser plasma — Thermal conduction

19 ABSTRACT (Continue on reverse if necessary and identify by block number)

A model for the development of the pronounced aneurism observed in the NRL LASER-HANE simulation experiment is presented. The model calculates the evaporative mass loss rate off the swept-up blast wave shell due to a thermal conduction front between the shell and the hot interior cavity. This front is limited to the segment of the shell where the self-generated magnetic fields are small. The thin-shell approximation is used to follow the nonlinear dynamics of the conductive and insulated segments, each of which is taken to be part of a spherical surface. The evaporating segment accelerates relative to the remaining part due to the decrease in its total mass and a rocket-like effect. For reasonable parameters the calculated time scale for appearance of the aneurism agrees with the experimental observations. Several suggestions are made for the future experiments to test the present model.

20 DISTRIBUTION/AVAILABILITY OF ABSTRACT	21 ABSTRACT SECURITY CLASSIFICATION
☒ UNCLASSIFIED/UNLIMITED ☐ SAME AS RPT ☐ DTIC USERS	UNCLASSIFIED
22a NAME OF RESPONSIBLE INDIVIDUAL J. L. Giuliani, Jr.	22b TELEPHONE (Include Area Code) (202) 767-3195
	22c OFFICE SYMBOL Code 4780

DD FORM 1473, 84 MAR 83 APR edition may be used until exhausted
All other editions are obsolete

SECURITY CLASSIFICATION OF THIS PAGE

CONTENTS

THERMAL EVAPORATION IN BLAST WAVES: A MODEL FOR ANEURISM FORMATION IN THE NRL LASER-HANE SIMULATION EXPERIMENT

I. INTRODUCTION

During the past two years the Plasma Physics Division at the Naval Research Laboratory has undertaken a program to develop a set of experiments which would simulate certain physical processes that are characteristic of a high altitude nuclear event (HANE). The program is under the auspices of DNA's Division of Atmospheric Effects and has the primary goal of a better understanding of the degradation of radar and communication transmissions through an atmosphere seeded by nuclear bursts. At the present time the experiment is initiated by irradiating a thin target foil with a neodymium laser. The subsequent rapid heating and disintegration of the target is followed by an expanding shock wave once the target debris couples to the background gas. Typical experimental parameters used thus far consist of an Al-foil less than 1 mm in diameter with a total mass of several tenths of a μgm, a 3.4 nsec laser pulse of total energy 4-400 Joules, and a mostly N_2 background gas of pressure 0.001-10.0 Torr threaded by a uniform magnetic field of either 0 or 800 Gauss strength.[1]

An important diagnostic has been dark-field shadowgraphy which gives a visual impression of the coupling region (or blast wave) as it expands. This process picks out steep density gradients in the image plane and permits multiple-time recordings on a single photograph. Stamper et al.[2] present several photographs which depict the coupling region at 52 and 96 nsec after the initial laser pulse, when the blast wave has expanded to about 1 cm from the target position. An unusual feature seen in the high ambient pressure shots is the development of an aneurism in the coupling shell: an outward protrusion from the nearly spherical blast wave toward the direction of the laser. The purpose of this report is to present a physical mechanism which may account for the development of this aneurism. Since this feature seems to ocur only in shots with a high ambient pressure (several Torr), the present theoretical model may have relevance for HANE phenomena at altitudes of 100 to 200 km.

Manuscript approved July 11, 1984.

II. OVERVIEW OF THE PHYSICAL MECHANISM

In this section we develop a schematic picture of the proposed physical mechanism responsible for the aneurism. A detailed account of the specific model equations will be given in the following section. Ripin et al.[3] have used the dark-field shadowgraphs to show that the radius of the coupling shell, R, expands as an adiabatic blast wave. The Taylor-von Neumann-Sedov self-similar solution shows that $R = \xi_o(E_o/\rho_o)^{1/5}t^{2/5}$ where E_o is the total laser energy, ρ_o is the ambient density, t is the time since the laser pulse and ξ_o is a constant of order unity. The basic physics of the blast wave can be readily found by assuming that all of the swept-up mass resides in a thin shell moving with the leading strong shock front while being pushed by the pressure inside the enclosed, hot cavity[4].

Basically, the proposed model complicates this simple picture by including a thermal condution front which forms on the inside edge of a small segment of the swept-up shell. The remainder of the shell is thermally insulated due to the magnetic fields which are generated at the target during laser burning and are subsequently carried out with the expanding plasma. Within the conduction front the electron heat flux from the hot cavity to the cooler shell is balanced by mass evaporation off the shell with the flow directed into the cavity. The mass unloading of the evaporating segment results in an acceleration relative to the insulated segment, assuming the cavity pressure is nearly uniform. Furthermore, the evaporating segment is accelerated by a rocket-like effect; the inward momentum carried off by the evaporative mass flow is balanced by forwad moving pressure waves driven into the swept-up shell. Of course, as the evaporating segment is accelerated forward, it sweeps up relatively more material and suffers an increase in the opposing ram pressure. Under the proper conditions we will show that this evaporating segment moves ahead of the remaining shell resulting in an aneurism-like feature.

A. Thermal Conduction

We first justify the model by estimating some relevant physical quantities. The effect of thermal conduction is central in the proposed model, but how important is thermal conduction in the experiment? Consider the total energy equation for the cavity,

$$\frac{\partial}{\partial t}\left(\frac{1}{2}\rho v^2 + \frac{1}{\gamma-1}p\right) + \vec{\nabla}\cdot\left[\vec{v}\left(\frac{1}{2}\rho v^2 + \frac{\gamma}{\gamma-1}p\right) + \vec{q}\right] = 0 \qquad (1)$$

We can neglect radiative losses since the analysis[3] of the present experiment indicates that the total energy with the blast wave is constant. The heat flux is predominantly carried by the electrons, so $\vec{q} = -\kappa_e(T)\,\vec{\nabla}T$ where $\kappa_e(T) = KT^{5/2}$ and $K = 1.4 \times 10^8$ ergs $cm^{-1}sec^{-1}$ $eV^{-7/2}$. The constant K was calculted from Braginskii[5] for a Coulomb logarithm of 10 and a charge per ion in the cavity $Z_c = 5$. Let L_T be the temperature scale height, $L_T = T/|\vec{\nabla}T|$, then

$$|q_e| \sim 6.5 \times 10^{16}\left(\frac{T_c}{300eV}\right)^{7/2}\left(\frac{cm}{L_T}\right)\frac{ergs}{cm^2\,sec}, \qquad (2)$$

where T_c is a characteristic cavity temperature. The 300 eV estimate for T_c was based on the following considerations. The high sound speed within the cavity implies a nearly uniform cavity pressure p_c and the conservation of total energy, together with an estimate of the postshock gas velocity, leads to the relation $p_c \sim p_s/2$, where p_s is the shell pressure[4]. Hence,

$$\frac{T_c}{T_s} \sim \frac{1}{2}\frac{\rho_s}{\rho_c}\frac{1 + Z_s}{1 + Z_c}, \qquad (3)$$

where Z_s is the mean charge per ion in the shell. The mean mass per particle, μ, has been replaced by $m_i/(1 + Z)$, with m_i the mass of a Nitrogen ion. The measured[6] values at the time of aneurism formation are $T_s \sim 15eV$, $Z_s \sim 3$ and $\gamma_s \sim 1.2$ implying $\rho_s/\rho_o \sim 11$, where ρ_o is the ambient density. Since most of the swept up mass resides in the shell, $\rho_s/\rho_c \gg 11$. In our calculations we will consider the set of values $T_c/T_s = (10,20,30)$ with the middle one corresponding $T_c = 300$ eV and $\rho_s/\rho_c = 60$.

Let us now estimate the enthalpy flux $\gamma vp/(\gamma - 1)$ in the cavity. The kinetic energy flux $\rho v^3/2$ in the energy equation (1) is negligible due to the low cavity density. Again using $p_c \sim p_s/2$

$$\frac{\gamma}{\gamma-1}pv \sim 7.2 \times 10^{14}\,\frac{1 + Z_s}{Z_s}\left(\frac{n_{e,s}}{3 \times 10^{18}cm^{-3}}\right)\left(\frac{T_s}{15eV}\right)\left(\frac{v_c}{10^7 cm/sec}\right)\frac{ergs}{cm^2\,sec}, \qquad (4)$$

where $\gamma = \gamma_c = 5/3$ and $3 \times 10^{18} cm^{-3}$ and $10^7 cm\ sec^{-1}$ are a typical electron density and shell velocity, respectively, for the high pressure shots[6]. Clearly the approximately measured enthalpy flux, Eq. (4), is much less than the estimated heat flux, Eq. (2) for any reasonable L_T ($\lesssim$1cm) . A similar result holds, though to a lesser degree, even if the heat flux is saturated. Saturation of the heat flux will be discussed more fully in section III. Thus the expansion of the cavity should be more nearly isothermal rather than adiabatic as in the Taylor-von Neumann-Sedov self-similar solution.

B. Magnetic Fields

Since the thermal conductivity perpendicular to the magnetic field can be smaller than along the field it is important to investigate the topology and strength of the magnetic field in the experiment. Consider the case where there is no ambient magnetic field. According to Kacenjar et al.[7] a magnetic field of 100 to 200 Gauss was still detected as the shell crossed the first magnetic probe located 1 cm from the symmetry axis and R = 1 cm from the target. A second measurement at the same offset, but R = 3 cm from the target found that the field strength near the shell had decreased to less than 20 Gauss. The orientation of the magnetic probe indicated that the field was azimuthal, i.e., field lines circled the symmetry axis. The presence of this field agrees with the theoretical model of magnetic field generation through the thermoelectric effect at the target surface during laser burning[8-10]. If this self-generated magnetic field is carried outward by the debris, it would decrease as $1/R^3$, consistent with the above measurements. This suggests that the magnetic field strength is $\gtrsim$ 1 kilogauss when $R \gtrsim 1$ cm, where the aneurism appears to start growing. Actually, this estimate is a lower limit since the magnetic probe may not resolve the magnetic field structure and the probe, which is encased in quartz tube to prevent space charging effects, requires the diffusion of the field out of the gas for a positive detection.

Thus, we adopt the estimate of 1 kG for the off-axis self generated magnetic field strength when $R < 1$ cm and an azimuthal orientation. The topology of such a field requires that it vanish along the symmetry axis. (A schematic diagram of the evolution of the blast wave is shown in Figure

1). In the off-axis portion of the shell the heat flux is perpendicular to the field and is thereby reduced relative to that in the segment of the shell along the symmetry axis where there is no field. We can quantitatively estimate this effect by using the approximation $\kappa_\perp \sim \kappa_\parallel/[1 + (\omega\tau)_e^2]$, where ω_e is the electron cyclotron frequency and τ_e is the electron collision time. The correct relation is more complicated[5], but the above simple one does have the proper dependence in the extreme limits. Using the previous estimates for the shell parameters one finds

$$(\omega\tau)_{e,s} \sim 0.01 \frac{B(kG)}{Z_s} \left(\frac{T_s}{15\ eV}\right)^{3/2} \left(\frac{3 \times 10^{18} cm^{-3}}{n_{e,s}}\right), \qquad (5)$$

which means that in the shell $\kappa_\perp \sim \kappa_\parallel$.

However, the field cannot remain in the shell. The magetic Reynolds number of the shell is

$$R_{M,s} = \frac{4\pi}{c^2} \sigma_\perp L_M v \sim \frac{73}{Z_s} \left(\frac{L_M}{cm}\right) \left(\frac{v_s}{10^7 cmsec^{-1}}\right) \left(\frac{T_s}{15eV}\right)^{3/2}, \qquad (6)$$

where $\sigma_\perp$ is the perpendicular electrical conductivity and L_M is the magnetic length scale. Using the shell thickness $L_s \lesssim 0.03$ cm for L_M and $Z_s \sim 3$, one finds $R_{M,s} < 1$. This implies that the field will diffuse out of the shell. Ahead of the shell R_M remains < 1 due to the small temperature and velocity, and a broad zone with a gentle compression of the magnetic field is formed. On the other hand, as the field diffuses back into the cavity it experiences a rapid increase in the temperature. The scale length of the diffusion region in the cavity where $R_{M,c} < 1$ is given by

$$L_M < 1.5 \times 10^{-4} Z_c \left(\frac{10^7 cmsec^{-1}}{v_c}\right) \left(\frac{300\ eV}{T_c}\right) cm , \qquad (7)$$

which is much less than the radius of the shell. Hence the field will stop diffusing once it moves back into the cavity while it will readily move ahead of the blast wave (see Figure 1c). This picture is verified by the temporal behavior of the field strength as measured by a stationary probe

in the experiments with an ambient magnetic field[7]. For the field in the the cavity one finds

$$(\omega\tau)_{e,c} \sim 70.0 \frac{B(kG)}{Z_c}\left(\frac{T_c}{300\ eV}\right)^{3/2}\left(\frac{5 \times 10^{16} cm^{-3}}{n_{e,c}}\right) . \qquad (8)$$

Thus away from the symmetry axis, the field resides just inside the shell and $\kappa \sim \kappa_\perp << \kappa_\parallel$, while along the axis $B \sim 0$ and $\kappa \sim \kappa_\parallel$. The effects of an ambient magnetic field will be briefly discussed in the last section.

C. Evaporative Mass Loss

Given that thermal evaporation is confined to a small segment of the shell the final question is how significant is the evapaorative mass loss. We model the evaporative process as a quasi-steady thin, i.e., planar, conduction front at the rear of the dense swept-up shell. Let $\hat{v}$ be the gas velocity relative to the conduction front. For subsonic flow one obtains from Eq. (1),

$$(\rho\hat{v})\frac{\gamma_c}{\gamma_c - 1}\frac{T_c}{\mu_c} \sim \kappa_e(T_c)\frac{dT}{dr} \qquad (9)$$

where $\mu_c = m_i/(1 + Z_c)$ is the mean mass per particle in the cavity. Following the nomenclature prior to Eq. (2) we compare

$$\frac{\text{evaporative mass loss rate}}{\text{swept-up mass gain rate}} = \frac{\rho\hat{v}}{\rho_o \dot{R}} \sim \frac{\gamma_c - 1}{\gamma_c}\frac{m_i}{1 + Z_c}\frac{KT^{5/2}}{\rho_o \dot{R}}\frac{1}{L_T} ,$$

$$= 6.6\ \left(\frac{10^{18} cm^{-3}}{n_o}\right)\left(\frac{10^7 cm\ sec^{-1}}{\dot{R}}\right)\left(\frac{T_c}{300\ eV}\right)^{5/2}\left(\frac{cm}{L_T}\right), \qquad (10)$$

where $\dot{R}$ is the velocity of the shell. This result means that evaporation can significantly reduce the mass in the conductive segment of the shell resulting in a protuberance (see Figure 1d). A more realistic estimate of the ratio will depend on the additional effects of a staurated heat flux, an increase in the mass gain rate as the shell segment accelerates forward, and a temporal decrease in the cavity's temperature.

III. MODEL EQUATIONS

A. Geometry and Nomenclature

Now that the general scenario of the proposed physical mechanism for the development of the aneurism has been presented, we will develop a set of more detailed equations to model the evaporative effects only. The topology and strength of the magnetic field is not calculated here; we assume it has the topology described in section II. The specific geometry is given in Figure 2. Thermal evaporation occurs within a sector 2θ, while outside of this sector the shell is assumed to be insulated by the azimuthal self-generated magnetic field. We will use the "thin-shell" approximation with R_s' being the radius of the insulated shell segment, and R_s the radius of the evaporating segment. Primed quantities will aways refer to the former segment and a subscript s denotes shell referenced values. We will neglect the detailed shape of the protrusion and consider the evaporating segment to be part of spherical surface. This of course greatly simplifies the calculation by reducing the model equations to one spatial dimension; however, it allows one to study the nonlinear physical processes acting to generate the protrusion. M_s and M_s' are the masses of the respective sections of the shell, and v_s and v_s' the gas velocities in the lab frame. The shock front on the outside edge of the swept-up shell will be taken to be a strong adiabatic shock. Hence we can use the relations

$$\frac{\rho_s}{\rho_o} = \frac{\gamma_s + 1}{\gamma_s - 1}, \quad v_s = \frac{2}{\gamma_s + 1}\dot{R}_s, \quad p_s = \frac{2}{\gamma_s + 1}\rho_o \dot{R}_s^2, \quad \frac{T_s}{\mu_s} = \frac{(\gamma_s - 1)}{(\gamma_s + 1)^2}\dot{R}_s^2 \qquad (11)$$

where $\dot{R}_s = dR_s/dt$, γ_s and μ_s are the specific heat ratio and mean mass per particle in the shell, respectively, and ρ_o is the ambient density.

B. Dimensional Form

In our model the total energy E_o is conserved, i.e., there are no radiative losses, and the cavity temperature and shell pressure are approximated as uniform. The total energy is the sum of the cavity's internal energy and the kinetic as well as internal energy in the two shell segments:

$$E_o = \frac{1}{\gamma_c - 1}\frac{4}{3}\pi\,[R_s'^3\cos^2(\tfrac{1}{2}\theta) + R_s^3\sin^2(\tfrac{1}{2}\theta)]p_c$$

$$+ \tfrac{1}{2}M_s v_s^2 + \tfrac{1}{2}M_s' v_s'^2 + \frac{1}{\gamma_s - 1}4\pi R_s^2 \Delta R p_s + \frac{1}{\gamma_s - 1}4\pi R_s'^2 \Delta R' p_s' . \quad (12)$$

The kinetic energy of the cavity material can be neglected due to its low density and small velocity. The presence of a conduction front does not alter the total energy equation since it only acts to exchange energy from internal to kinetic. The internal energy of the shell is typically negelected[4], though actually it equals the shells kinetc energy. The equality follows from the thin-shell approximation which gives $M_s = 4\pi R_s^2 \Delta R_s \rho_s$, and Eq. (11). The resulting total energy equation can then be written as

$$E_o = \frac{1}{\gamma_c - 1}\frac{4\pi}{3}\,[R_s'^3\cos^2(\tfrac{1}{2}\theta) + R_s^3\sin^2(\tfrac{1}{2}\theta)]p_c$$

$$+ M_s v_s^2 + M_s' v_s'^2 \quad . \quad (13)$$

The total momentum equation represents a balance between the rate of change of the momentum of the shell and the pressure force supplied by the cavity. Since there are two shell segments one has

$$\frac{d}{dt}(M_s' v_s') = 4\pi R_s'^2 \cos^2(\tfrac{1}{2}\theta) p_c \quad . \quad (14)$$

and

$$\frac{d}{dt}(M_s v_s) = 4\pi R_s^2 \sin^2(\tfrac{1}{2})\ (p_c + p_{evp}) \quad . \quad (15)$$

The additional pressure p_{evp} in Eq. (15) is due to the rocket-like effect as mass evaporates off the shell segment and flows backward into the cavity. Its value will be developed when we discuss the equations describing the conduction front.

The total masses in the different segments of the swept-up shell are

$$M_s' = \frac{4\pi}{3} R_s'^3 \rho_o \cos^2(\tfrac{1}{2}\theta), \quad (16)$$

and

$$M_s = \frac{4\pi}{3} R_s^3 \rho_o \sin^2(\tfrac{1}{2}\theta) - M_{evp} \ , \tag{17}$$

where M_{evp} is the total mass which has been evaporated from the conducting segment of the shell. Again its value will be discussed below.

Let us pause in the development of the model equations and consider the solutions in the purely adiabatic case, i.e., $\theta = 0$. The results will be required as initial conditions prior to the onset of thermal evaporation over a segment of the shell. Combining Eqs. (11), (13), (14), and (16), one readily finds

$$R_s = \xi_o \left(\frac{E_o}{\rho_o}\right)^{1/5} t^{2/5} \ , \tag{18}$$

$$\xi_o^5 = \frac{75}{16\pi} \frac{(\gamma_c - 1)(\gamma_s + 1)^2}{[\gamma_s + 1 + 4(\gamma_c - 1)]} \ , \tag{19}$$

and

$$p_c = \frac{1}{\gamma_s + 1} \rho_o \dot{R}_s^2 = \frac{1}{2} p_s \tag{20}$$

These results agree with Ripin *et al*[3]. If the shell's internal energy had been neglected the quantity $4(\gamma_c - 1)$ in Eq. (19) would be replaced by $2(\gamma_c - 1)$. Then for $\gamma_s = \gamma_c$ one recovers the formula given in Zel'dovich and Raizer[4].

In order to include the effects of thermal evaporation we need an equation for the cavity temperature T_c, which is assumed to be uniform except in the conduction front. The total energy equation will be used to evaluate the cavity pressure p_c and by the equation of state for an ideal gas,

$$p_c = \frac{3(M_{c,ad} + M_{evp})}{4\pi[R^3 \cos^2(\tfrac{1}{2}\theta) + R_s \sin^2(\tfrac{1}{2}\theta)]} \frac{T_c}{\mu_c} \tag{21}$$

In the absence of evaporative mass gain to the cavity, $M_{c,ad}$ is the total mass in the cavity under adiabatic conditions. This mass is negligible

compared to that in the swept-up shell, but it cannot be zero since the cavity must have a finite temperature. The Taylor-von Neumann-Sedov solution gives a cavity density which depends only on the self-similar variable, r/R_s'. Hence the total mass in the cavity increases as $R_s'^3$, i.e., $M_{c,ad}/\rho_o R_s'^3$ is constant, and the porportionality factor depends on the artificial demarcation in r/R separating the cavity from the shell. We can avoid this problem noting that for adiabatic expansion

$$\frac{p_c}{p_s} = \left(\frac{3M_{c,ad}}{4\pi\rho_o R_s'^3}\right)\frac{\gamma_s - 1}{\gamma_s + 1}\frac{\mu_s T_c}{\mu_c T_s} \tag{22}$$

from Eqs. (11) and (21). During this phase, p_c/p_s is fixed by the energy equation (Eq. [20]) and a choice of the parameter T_c/T_s gives an effective value for $M_{c,ad}/\rho_o R_s'^3$. We will assume that this ratio remains constant after evaporation begins. This approximation is reasonable in the case that θ is a small angle, resulting in a small change to the adiabatic solution, and is irrelevant in the case that the whole shell is subject to evaporation, since M_{evp} quickly exceeds $M_{c,ad}$.

Finally, we need to formulate a set of equations for the conduction front so that M_{evp} and p_{evp} can be explicitly evaluated. We use the approach given in section II, i.e, the conduction front is a thin, planar shell at the inside edge of the swept-up shell and in quasi-steady equilibrium. Let $\rho\hat{v}$ be the mass flow rate through the conduction front with $\hat{v}$ the gas velocity relative to the front. Then setting

$$j = \frac{\rho\hat{v}}{\rho_o \dot{R}_s}, \tag{23}$$

we have

$$\dot{M}_{evp} = j4\pi R_s^2 \dot{R}_s \rho_o \sin^2\left(\frac{1}{2}\theta\right). \tag{24}$$

Conservation of momentum through the conduction front is simply,

$$\rho\hat{v}^2 + p = p_s + \rho_s \hat{v}_s^2, \tag{25}$$

with $\rho_s = \rho_o (\gamma_s + 1)/(\gamma_s - 1)$ since the leading shock is taken everywhere to be a strong adiabatic one. By momentum conservation the additional

pressure on the evaporating segment of the shell due to the rocket-like effect is

$$p_{evp} = \rho_s \hat{v}_s^2 = j^2 \frac{\gamma_s - 1}{\gamma_s + 1} \rho_o \dot{R}_s^2 \ . \tag{26}$$

This pressure prevents the conduction front from overrunning the leading shock.

For the energy equation we balance the heat flux into swept-up shell against the energy carried by the mass flux off the shell. From Eq. (1) we have

$$\frac{1}{2}\rho \hat{v}^3 + (\rho \hat{v}) \frac{\gamma}{\gamma-1} \frac{T}{\mu} = -q = \frac{\kappa_e(T)}{1 + \frac{\kappa_e(T)}{q_{sat}} \left|\frac{dT}{dz}\right|} \frac{dT}{dz}, \tag{27}$$

where $z = 0$ at the interface between the conduction front and the swept-up snell and increases toward the cavity. The generalized heat flux q in eq. (27) is an approximate representation for the limitation on the heat flux when the electron mean free path ℓ_e is on the order of the temperature length L_T. Under this condition the electron distribution function is far from Maxwellian, the classical relation $\vec{q} = -\kappa_e(T) \vec{\nabla} T$ breaks down, and the maximum, i.e., saturated, heat flux is that given by the free-streaming limit:

$$q_{sat} = \alpha n_e T \left(\frac{T}{m_e}\right)^{1/2} \ . \tag{28}$$

The parameter α has been determined to be ~ 0.06 from Fokker-Planck simulations and experiments[11] It is instructive to express the conductivity coefficient in terms of the electron mean free path:

$$\kappa_e(T) = \frac{f(Z)}{\sqrt{3}} n_e \left(\frac{T}{m_e}\right)^{1/2} \ell_e \ ,$$

$$\ell_e = \frac{3^*}{4} \sqrt{\frac{3}{2\pi}} \frac{T^2}{n_e Z_e^4 \ell n \Lambda} \ , \tag{29}$$

and f(z) is a function tabulated by Braginskii[5]. Rewriting Eq. (27) via Eqs. (28) and (29) gives

$$\frac{1}{2}\rho\hat{v}^3 + (\rho\hat{v})\frac{\gamma}{\gamma-1}\frac{T}{\mu} = \frac{f(Z)n_e T^{3/2}(\frac{\ell_e}{T}\frac{dT}{dz})/\sqrt{3m_e}}{1 + \frac{f(z)}{\alpha\sqrt{3}}(\frac{\ell_e}{T}|\frac{dT}{dz}|)} \tag{30}$$

which explicitly displays the dependence of the heat flux on the different length scales.

C. Non-dimensionalization of the Dynamic Equations

It is convenient to write the equations in dimensionless form prior to obtaining solutions. For the total mass, momentum and energy equations we choose a fudicial time t_1 prior to which the expansion is entirely adiabatic. The value of t_1 is determined by the solutions for the structure of the conduction front. At time t_1 one has from Eqs. (18), (19), and (20),

$$R_1 = \xi_o(\frac{E_o}{\rho_o})^{1/5} t_1^{2/5}, \quad \dot{R}_1 = \frac{2}{5}\frac{R_1}{t_1},$$

$$M_1 = \frac{4}{3}\pi R_1^3\rho_o, \quad p_{c,1} = \frac{4}{25(\gamma_s+1)}\rho_o(\frac{R_1}{t_1})^2 \tag{31}$$

We now define the dimensionless variables as

$$t = \tau t_1, \quad R_s \equiv \lambda R_1, \quad \dot{R}_s \equiv \lambda' R_1, \quad p_c \equiv \eta p_{c,1}$$

$$M_{evp} \equiv \omega M_1 \sin^2(\tfrac{1}{2}\theta), \quad M_{c,ad} \equiv \varepsilon_M M_1 \lambda'^3,$$

$$T \equiv \zeta T_s, \quad n_e \equiv \nu n_{e.s}, \quad \rho\hat{v} \equiv j\rho_o\dot{R}_s \tag{32}$$

Note that the last three definitions are written in terms of the evaporating shell variables. They will be used to analyze the conduction front. Also recall from Eq. (22) that ε_M is taken to be a constant determined by an initial choice of

$$(T_c/T_s)_1 = (T_c/T_s')_1 = \zeta_{c,1},$$

where

$$\frac{1}{2} = \varepsilon_M \frac{\gamma_s - 1}{\gamma_s + 1} \frac{1 + Z_c}{1 + Z_s} \zeta'_{c,1} \cdot \tag{33}$$

Equation (32) gives in turn

$$M'_s = M_1 \cos^2(\tfrac{1}{2}\theta)\ \lambda'^{-3},\ M_s = M_1 \sin^2(\tfrac{1}{2}\theta')(\lambda^3 - \omega),$$

$$v'_s = \frac{2}{\gamma_s + 1} \frac{R_1}{t_1} \frac{d\lambda'}{d\tau},\ v_s = \frac{2}{\gamma_s + 1} \frac{R_1}{t_1} \frac{d\lambda}{d\tau} \cdot \tag{34}$$

The equations for energy (Eq. [13]) and momentum (Eqs. [14] and [15]) can now be written, respectively, as

$$\frac{2}{25} \frac{(\gamma_s + 4\gamma_c - 3)}{(\gamma_c - 1)} - \lambda'^{-3}(\frac{d\lambda'}{d\tau})^2 \cos^2(\tfrac{1}{2}) - (\lambda^3 - \omega)\ (\frac{d\lambda}{d\tau})^2 \sin^2\ (\tfrac{1}{2}\theta)$$

$$= \frac{2}{25}(\frac{\gamma_s + 1}{\gamma_c - 1})\ [\lambda'^{-3}\cos^2(\tfrac{1}{2}\theta) + \lambda^3 \sin^2(\tfrac{1}{2}\theta)]\eta\ , \tag{35}$$

$$\lambda'^{-3} \frac{d^2\lambda'}{d\tau^2} = [\frac{6}{25}\eta - 3\ (\frac{d\lambda'}{d\tau})^2]\lambda'^{-2}\ , \tag{36}$$

and

$$(\lambda^3 - \omega) \frac{d^2\lambda}{d\tau^2} = [\frac{6}{25}\ \eta + \frac{3}{2}(\gamma_s - 1)\ j^2(\frac{d\lambda}{d\tau})^2 - 3(\frac{d\lambda}{d\tau})^2]\lambda^2 + \frac{d\omega}{d\tau} \frac{d\lambda}{d\tau} \cdot \tag{37}$$

In the last equation we have used Eqs (26) and (31). Equation (24) for the rate of change of the evaporated mass transforms to

$$\frac{d\omega}{d\tau} = 3j\lambda^2 \frac{d\lambda}{d\tau} \cdot \tag{38}$$

Finally using Eqs. (11), (31), (32) the relation between the cavity pressure and temperature (Eq. [21] becomes

$$\eta = \frac{25}{2}\ \frac{\gamma_s - 1}{\gamma_s + 1} \frac{1 + Z_c}{1 + Z_s} [\frac{\varepsilon_M \lambda'^{-3} + \omega \sin^2(\frac{1}{2}\theta)}{\lambda'^{-3}\cos^2(\frac{1}{2}\theta) + \lambda^3 \sin^2(\frac{1}{2}\theta)}](\frac{d\lambda}{d\tau})^2 \zeta_c \cdot \tag{39}$$

The set of parameters is $\{\gamma_s, \gamma_c, Z_s, Z_c, \theta, \zeta_{c,1}\}$ and the set of unknowns is $\{\lambda, \lambda', d\lambda/d\tau, d\lambda'/d\tau, \omega, j\}$. Subject to the initial conditions at $\tau = 1$,

$$\lambda = \lambda' = 1, \frac{d\lambda}{d\tau} = \frac{d\lambda'}{d\tau} = \frac{2}{5}, \omega = j = 0 , \tag{40}$$

the system of equations (36), (37), and (38) can be integrated forward in time (τ) , using Eq. (35) to determine the cavity pressure (η) , once an expression for the evaporated mass loss rate (j) has been given. To do so we will need Eq. (39) and a solution of the structure of the conduction front.

IV. RESULTS

A. Solution for the Evaporative Mass Loss Rate

Let us begin by multiplying the momentum conservation Eq. (25) by p/p_s^2 to obtain

$$\frac{j^2(\rho_o \dot{R}_s)^2}{p_s^2}\frac{p}{\rho} + (\frac{p}{p_s})^2 = (\frac{p}{p_s})[1 + j^2(\frac{(\rho_o \dot{R}_s)^2}{\rho_s p_s}] .$$

From Eq. (11), $(\rho_o \dot{R}_s)^2/\rho_s p_s = (\gamma_s - 1)/2$, and one can now solve the quadratic equation for the pressure ratio:

$$\frac{p}{p_s} = \frac{1}{2}\left[1 + j^2\frac{\gamma_s - 1}{2} \pm \left\{(1 + j^2\frac{\gamma_s - 1}{2})^2 - 4j^2\frac{\gamma_s - 1}{2}(\frac{1 + Z}{1 + Z_s}\frac{T}{T_s})\right\}^{1/2}\right] . \tag{41}$$

Since j is limited to about 1 and $\gamma_s = 1.2$ from the experimental analysis[3], $\frac{1}{2}j^2(\gamma_s - 1) \ll 1$. The positive sign is then the proper choice to satisfy the boundary condition at the front of the conduction front where $\mu_s T/\mu T_s = 1$. Clearly, Eq. (41) constrains the mass flux giving approximately

$$j \leq \frac{1}{\left(\frac{\gamma_s - 1}{2}\frac{1 + Z}{1 + Z_s}\frac{T_c}{T_s}\right)^{1/2}} . \tag{42}$$

When the equality holds, the maximum value for the mass loss rate j_{max} corresponds to the maximum pressure drop through the conduction front. Note that although the temperature at the rear of the conduction front is

that of the cavity (T_c), the pressure at this point (p_2) is larger than p_c; once the evaporating segment accelerates relative to the adiabatic segment $p_s > p'_s$ giving $p_c \sim p'_s/2 < p_s/2 < p_s$. We surmise that the conduction front will adjust to maximize the pressure drop and hence also j. In the terminology of fluid combustion[12], the choice of the positive sign in Eq. (41) means that our conduction front is analogous to a deflagration reaction. The composite structure of a conduction front and a preceeding shock wave can be viewed as a deflagration initialed by a shock i.e., a detonation wave. Our assumption that $j = j_{max}$ is equivalent to the Chapman-Jouguet hypothesis.

The size of the conduction front is given by solving the energy equation through the conduction front, Eq. (30). To do this first scale z by the radius R_s ($z = y R_s$) and then combine Eqs. (29) and (32) to get

$$\frac{\ell_e}{T}\frac{dT}{dz} = \left\{\frac{3}{4}\sqrt{\frac{\overline{3}}{2\pi}}\frac{T_s^2}{n_{e,s}Ze^4\ell n\Lambda}\right\}\frac{\zeta}{\nu\zeta}\frac{d\zeta}{dy} \tag{43}$$

Except for the variation in the Coulomb logorithm and Z, the term in the curly braces is the ratio of the electron mean free path in the swept-up shell to R_s. Let us then rewrite Eq. (43) as

$$\frac{\ell_e}{T}\frac{dT}{dz} = \left(\frac{\ell_{e,s}}{R_s}\right)\frac{\zeta^2}{\nu\zeta}\frac{d\zeta}{dy}\,. \tag{44}$$

By using this equation and Eqs. (11) and (32), the energy equation (30) can be transformed to

$$\left(1 + \frac{\gamma - 1}{2}M^2\right)j = \frac{a\left(\frac{\ell_{e,s}}{R_s}\right)\zeta^{3/2}\frac{d\zeta}{dy}}{1 + b\left(\frac{\ell_{e,s}}{R_s}\right)\frac{\zeta^2}{\nu\zeta}\frac{d\zeta}{dy}} \tag{45}$$

where

$$a = \frac{Z_s f(Z)}{(1+Z)\sqrt{3}}\frac{\gamma - 1}{\gamma}\left[\frac{2m_i}{m_e(\gamma_s - 1)(1+Z_s)}\right]^{1/2},$$

$$b = \frac{f(Z)}{\sqrt{3}}, \tag{46}$$

and M is the adiabatic Mach number of the flow relative to the conduction front. We make several approximation in order to integrate equation (45). First we neglect the variation of Z through the conduction front and set Z equal to Z_c in Eqs. (42), (43), and (46). Second, we set $\gamma = \gamma_c = 5/3$. It is then reasonable to neglect the term $(\gamma - 1)M^2/2$ compared to unity. The Chapman-Jouguet condition for the conduction front has M reaching a maximum of one at the rear of the front and so this term is $< 1/3$. Finally we can write

$$\nu\zeta = \frac{n_e T}{n_{e,s}, T_s} = \frac{Z(1 + Z_s)}{Z_s(1 + Z)} \frac{p}{p_s}. \tag{47}$$

Before we noted that p/p_s drops from 1 to $\sim 1/2$ through the front and from Eq. (41) most of the change occurs near the rear. Thus we fix $\nu\zeta = 1$. The solution to Eq. (45) is now readily found to be

$$y = \left(\frac{\ell_{e,s}}{R_s}\right) \left[\frac{2a}{5j} (\zeta^{5/2} - 1) - \frac{b}{3}(\zeta^3 - 1)\right]. \tag{48}$$

The first property to note from this result is that at $\zeta = \zeta_c$, y must be less than unity in order to fit the conduction front within the blast wave radius R_s. Initially ζ has the constant value $\zeta_{c,1}$, while $\ell_{e,s}/R$ decreases. The evaporation process can begin once

$$\left(\frac{\ell_{e,s}}{R_s}\right)_1 < \left[\frac{2a}{5j} (\zeta_{c,1}^{5/2} - 1) - \frac{b}{3}(\zeta_{c,1}^3 - 1\right]^{-1}. \tag{49}$$

By a series of manipulations involving Eqs. (11) and (31) one finds

$$\frac{\ell_{e,s}}{R} = \left[3\sqrt{\frac{3}{2\pi}} \frac{m_i^3}{e^4 \ell n\Lambda} \frac{1}{Z_c^2(1 + Z_s)^2} \frac{(\gamma_s - 1)^3}{(\gamma_s + 1)^5}\right] \frac{\xi_o^3 E_o^{3/5}}{\rho_o^{8/5} t_1^{14/5}} \frac{1}{\lambda}\left(\frac{d\lambda}{d\tau}\right)^4. \tag{50}$$

We now identity t_1 with the turn-on time for evaporation. At this time $\lambda = 1$, $d\lambda/d\tau = 2/5$ and by using the relation $\rho_o(\text{gr cm}^{-3}) = 1.64 \times 10^{-6} p_o$ (Torr) we can convert Eq. (50) to practical units and explicitly define the initial time as

$$t_1(\text{nsec}) = 1.1 \times 10^2 \left[\frac{1}{Z_c^2(1 + Z_s)^2} \frac{(\gamma_s - 1)^3}{(\gamma_s + 1)^5}\right]^{5/14} \times$$

$$\frac{\xi_o^{15/14} E_o(\text{Joules})^{3/14}}{p_o(\text{Torr})^{8/14}} \left(\frac{R_s}{\ell_{e,s}}\right)_1^{5/14}. \tag{51}$$

The corresponding length is

$$R_1(\text{cm}) = 0.60 \left[\frac{1}{Z_c^2(1+Z_s)^2} \frac{(\gamma_s - 1)^3}{(\gamma_s + 1)^5}\right]^{1/7} \times$$

$$\frac{\xi_o^{\frac{10}{7}} E_o\ (\text{Joules})^{2/7}}{p_o\ (\text{Torr})^{3/7}} \left(\frac{R_s}{\ell_{e,s}}\right)_1^{1/7}. \tag{52}$$

We can further use Eq. (48) to determine a turn-off condition for evaporation. After evaporation begins, the size of the conduction front y_c, given by setting $\zeta = \zeta_c$ in Eq. (48), decreases rapidly. This is due to the decrease in T_c/T_s as the evaporating shell segment accelerates relative to the insulated segment. Since there is only a small mass addition into the cavity for small θ, T_c/T_s' remains nearly constant, T_s/T_s' increases, and hence T_c/T_s decreases. Furthermore $\ell_{e,s}/R_s$ decreases as evidenced by the form of Eq. (50). At some point y_c can become on the order of the electron mean free path in the cavity. The latter quantity is given by

$$\frac{\ell_{e,c}}{R_s} = \frac{\ell_{e,s}}{R_s} \frac{\zeta_c^2}{\nu_c}. \tag{53}$$

We have rather arbitrarily cut off conduction when y_c is twice this value. The aspect represents the fact that at this point electrons can freely stream from the cavity right into the swept-up shell. The resulting large anisotropy in the electron distribution is not accounted for in the present simple model for saturated conduction.

To summarize, the value of the cavity to shell temperature ζ_c is given by Eq. (39). The value of the mass evaporation rate (j) can then be computed using the equality in Eq. (42). If the size of the conduction front is less than R_s ($y_c < 1$), the calculated value of j is used in eq. (38). However, if the size of the front is less than twice the electron mean free path in the cavity, the value of j is set to zero. We note from eq. (42) that $j \propto \zeta_c^{-1/2}$. This is consistent with the form of equation (45) since the heat flux becomes more strongly saturated as the expansion proceeds.

B. Solution for the Evolution of the Aneurism

In Figure 3 we present the results for three calculations. For all angels we found that the expansion of the insulated segment of the shell was close to the purely adiabatic law, $\lambda = \tau^{2/5}$. This relation is shown as a solid line in the graph. The position of the evaporating segment, i.e., the aneurism, is represented by the different symbols corresponding to the different choices for the parameters which are listed in Table 1. The time and length units, t_1 and R_1, are calculated from Eqs. (49), (51), and (52) for different initial choices of $\zeta_{c,1} = (T_c/T_s)_1$. These units are normalized to $E_0 = 10$ Joules and $p_o = 5$ Torr, which are typical values for the high pressure experiments.

The calculations do not indicate a significant angle dependence of the expansion of the protuberance for θ within a factor of two of 30^o. However, changes in the parameters Z_c and/or γ_c do result in a wide variation in the shape of the solution curve for R_s/R_1, as well as changes in the time and length units.

V. SUMMARY AND DISCUSSION

In this report we have suggested a new physical mechanism for the development of the aneurism observed in the laser-Hane experiment. The essential feature of the model is the formation of a thermal conduction front on the inside surface of the swept-up blast wave shell. The conduction front is limited to a small segment about the symmetry axis of the incoming laser beam due to an azimuthal magnetic field carried outward by the shell. The field is generated at the target during the laser burning. Within the conduction front the thermal heat flux from the cavity into the shell is balanced by an evaporative mass flow from the shell back into the cavity. The major analysis of this report used the thin-shell approximation to model the rocket-like acceleration of the evaporating segment ahead of the insulated part of the blast wave shell.

Below are a number of points on the implication and limitations of the present model for the development of the aneurism.

1.) Figure 3 and Table 1 clearly shows that the growth of the protuberance is faster the smaller the value of $(T_c/T_s)_1$. This feature is contrary to one's expectation in a mechanism where thermal conduction is

important. However this expectation is based on the use of the classical thermal conductivity coefficient. Let us use Eq. (48) to determine j;

$$j = \frac{\frac{2}{5}\ a\left(\frac{\ell_{e,s}}{R_s}\right)\left(\zeta_c^{5/2} - 1\right)}{y_c + \frac{b}{3}\left(\frac{\ell_{e,s}}{R_s}\right)\left(\zeta_c^{3} - 1\right)} \ . \qquad (54)$$

We can effectively keep the heat flux from strongly saturating by maximizing the size of the conduction front, i.e., setting $y_c = 1$. Then as $(\ell_{e,s}/R_s)$ decreases (roughly as $\tau^{-14/5}$ from Eq. [50], the conduction front would become less and less saturated and the evaporation rate would have the expected behavior on the temperature ratio $j \propto \zeta_c^{5/2}$. The resulting value of j would be very small after τ reaches a few. However, this classical model is inconsistent. The conduction front, which would extend over the whole cavity, has a negligible pressure drop, contrary to the known relation $p_c \sim 1/2\ p_s$. In the pressure model, this pressure drop enforces the Chapman-Jouguet condition for the conduction front. This condition is equivalent to the equality in Eq. (42), which gives rise to the calculated dependence in T_c/T_s. As a consequence, Eq. (54) shows that $y_c \ll 1$ and the heat flux is highly saturated through the front.

2.) As a test of the present model we solved the system of equations with $2\theta = 2\pi$, i.e., we modeled an "isothermal" blast wave. Independent of the parameter $(T_c/T_s)_1$, the results were that after the evaporation process commenced, the radius of the shell R_s was 1.09 times larger than the radius of the Taylor-von Neumann-Sedov, purely adiabatic, blast wave, R_{ad}. This compares favorably with the detailed self-similar solution[13,14] for an isothermal blast wave where $R_s = 1.08\ R_{ad}$.

3.) We note that the time scale for turn-on of the evaporation process (Eq. [51]) scales as $E_o^{3/14} p_o^{-8/14}$. This is consistent with the experimental observation that the aneurism does not occur, or is delayed, in high energy, low pressure shots[2]. The parameters in Table 1 for the calculations in Figure 3 give time scales for the appearance of the aneurism that are within a factor of two of the experimental values. However the experiment shows a wide variety in the structure of the aneurism; some grow, some grow then decay, while others appear turbulent. Undoubtably there are a large number of factors which effect the dynamics

of the aneurism. The model proposed here has only attempted to analyze a single potential mechanism in the nonlinear regime.

4.) One of the most serious drawbacks of the present calculation is that it is limited to one dimension. The two dimensional aspects of tangential flow in the aneurism and oblique shock could significantly alter the evolution of the proturbance in our model.

5.) A second drawback in the model is the neglect of the evolution of the topology and magnitude of the self-generated magnetic field. We have also ignored the presence of an ambient magnetic field. For the parameters of the present experiment, the ambient field would have no dynamic effect on the growth of the aneurism; the total magnetic energy of a 800 Gauss field in a sphere of radius 1 cm is ~ 0.01 Joules which is far less than the several Joules imparted by the laser to the target. This conclusion is consistent with the claim of the experimental group that the aneurism shows no dramatic change whether the ambient field is on or off (though see Brecht[15]). However, one interesting feature also noted by the group was that the aneurism sometimes appears to form slightly of the symmetry axis. A possible explanation for this feature in the context of the present model is a follows. When the ambient field was on it was directed into or out of the plane depicted in Figure 1. As the shell sweeps over some of the ambient field, a cancellation with the self-generated field could result in a negligible magnetic field at an off-axis position thereby generating an off-axis aneurism. This position would depend on the orientation of the ambient field. A review of the present data might be relevant in this matter. We also suggest that future runs of the experiment be made with the ambient magnetic field in the plane of Figure 1 to see if, and how, the aneurism is affected.

6.) A final limitation in the model was the approximate calculation for the structure of the conduction front. We assumed a quasi-steady state, neglecting variations in the ionization level Z, and ignored other physical aspects such as temperature non-equipartition between the ions and electrons. Despite these limitations we can make two general comments. If evaporation is acting to drive the observed aneurism there would result a mass flow off the shell into the region behind the aneurism. This mass flow is much larger than the flow off the shell from the adiabatic, i.e., not evaporating, segments. One might expect to find a higher gas density

behind the aneurism than behind the other parts of the blast wave. This is in fact the observed case, at least for the electrons in the single shot where an interferogram was obtained[16]. This model would also predict that the gas near the aneurism would have a higher temperature than the gas in the other segments of the blast wave. This is due to the relative acceleration of the evaporating segment leading to a higher temperature in the shell and to the heating within the conduction front. It might be possible in future experiments to measure the temperature near the aneurism using spectroscopy.

Acknowledgments

I gratefully thank fruitful discussions with Joe Huba, Barry Ripin, John Stamper, Ed McLean, Jacob Grum, Steve Kacenjar and Mike Keskinen of the NRL Plasma Physics Division. This research was supported by the Defense Nuclear Agency.

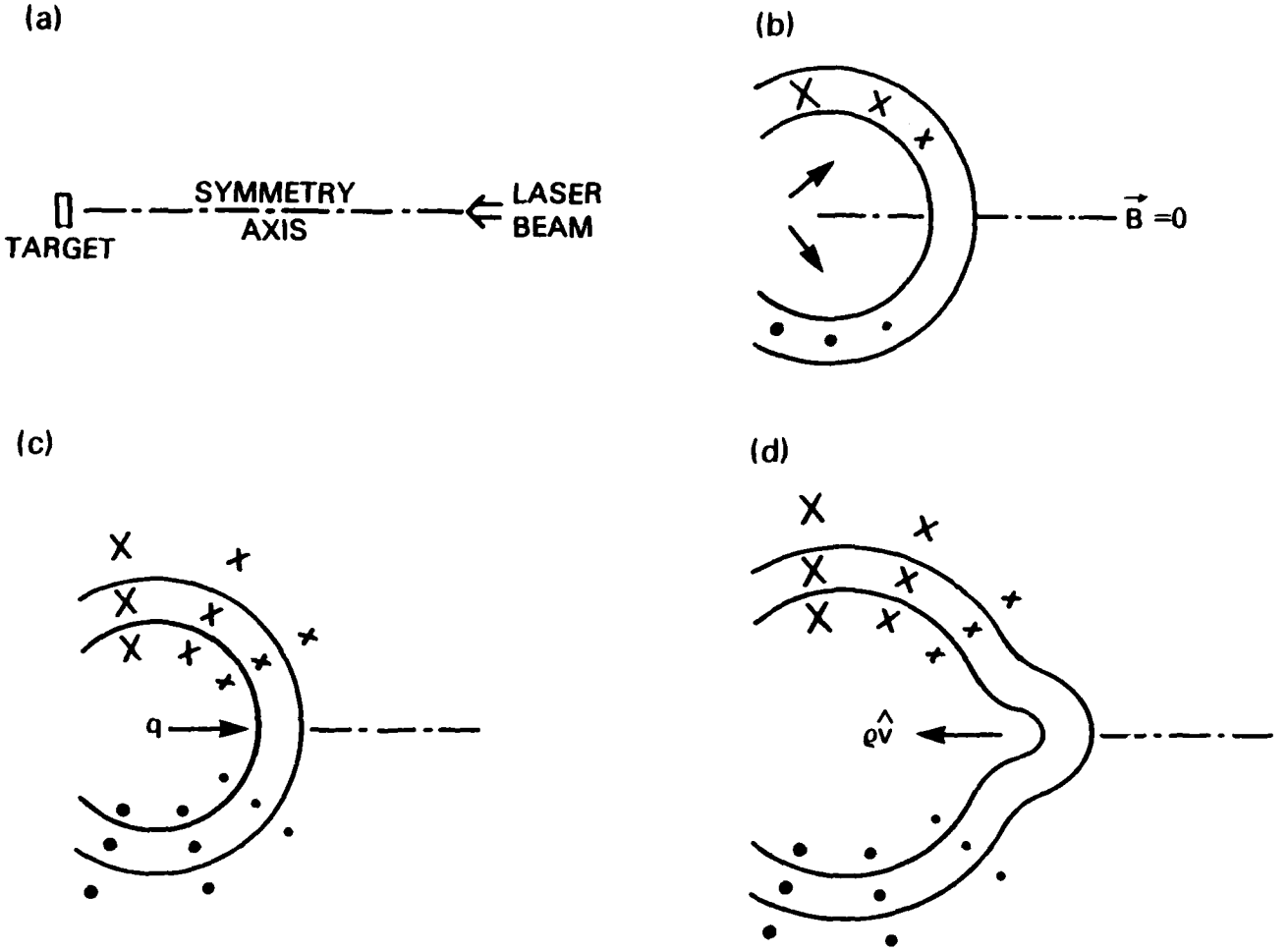

Fig. 1) Schematic cartoon of the proposed physical mechanism leading to the development of an aneurism in the blast wave. The crosses and dots represent the magnetic field into and out of the plane of the diagram. A heat flux $\vec{q}$ acts along the thermally unisulated section of the blast wave shell. The evaporative mass flux $\hat{\rho v}$ then leads to the aneurism development. Further aspects are explained in section II of the text.

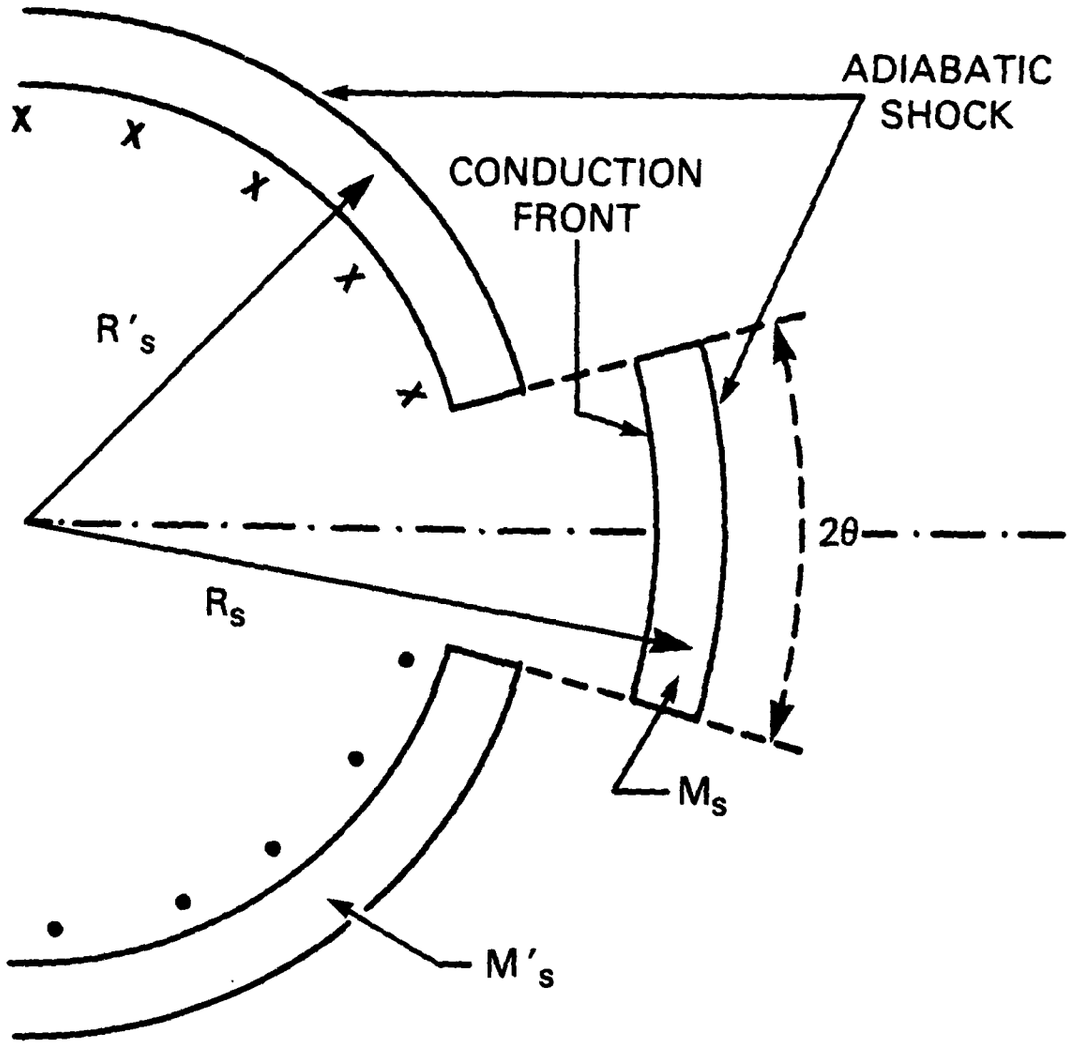

Fig. 2) Geometrical definitions used in the thin-shell approximation for the dynamic equations.

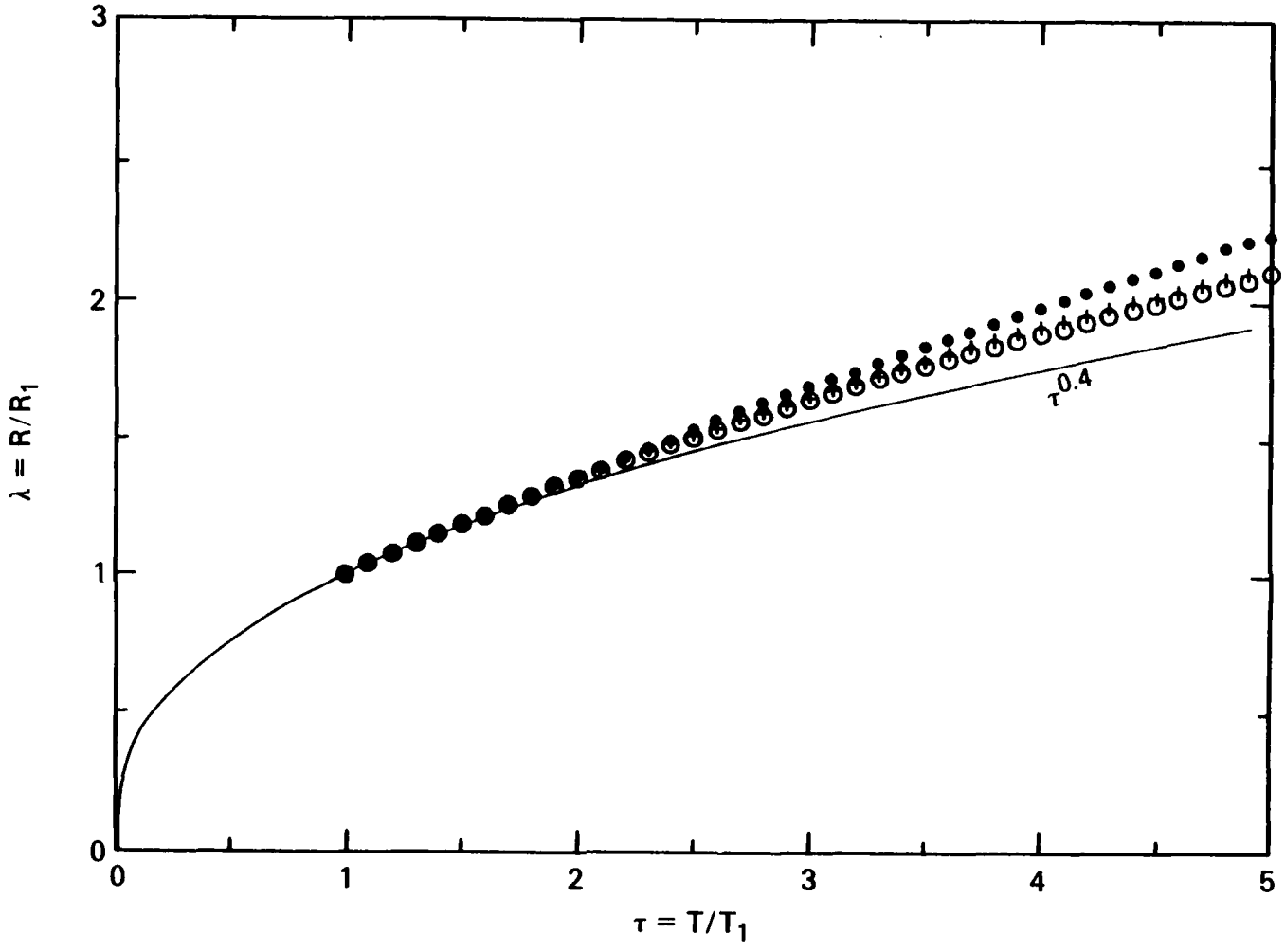

Fig. 3) Plot of the dimensionless radius R/R_1 of the evaporating segment,i.e., the aneurism (given by the different symbols), and the radius of the insulated segment (solid line) as a function of the dimensionless time t/t_1. The scaling and parameters for the different solutions are listed in Table 1.

Table 1 — Data for Figure 3

$$t_1 = a \left(\frac{E_o}{10 \text{ Joules}}\right)^{3/14} \left(\frac{5 \text{ Torr}}{P_o}\right)^{8/14} \text{ nsec}$$

$$R_1 = b \left(\frac{E_o}{10 \text{ Joules}}\right)^{2/7} \left(\frac{5 \text{ Torr}}{P_o}\right)^{3/7} \text{ cm}$$

γ_s	γ_c	Z_s	Z_c	$(T_c/T_s)_1$	θ^o	$(\ell_{e,s}/R_s)_1$	a	b	symbol
1.2	1.67	3	3	30	30	1.2E6	55.	0.54	0
1.2	1.67	3	5	20	30	3.4E5	36.	0.44	+
1.2	1.67	3	5	10	30	4.3E4	17.	0.32	*

REFERENCES

1. B.H. Ripin, J. Grun, S. Kacenjar, E.A. McLean, and J.A. Stemper, NRL Memo Report #5268, "Introduction to the Laser-Hane Experiment and Summary of Low-Pressure Interaction Results," (1984). (AD A138 945)
2. J.A. Stamper, B.H. Ripin, E.A. McLean, and S.P. Obenschain, NRL Memo Report #5278, "Optical Imaging of a Coupling Region Between Inter-Streaming Plasmas," (1984). (AD A-139 191)
3. B.H. Ripin, J.A. Stamper, and E.A. McLean, NRL Memo Report #5279, "Blast Wave Analysis of High-Pressure Coupling Shells." (1984). (AD-A139 687)
4. Ya. B. Zel'dovich and Yu P. Raizer, Physics of Shock Waves and High Temperature Hydrodynamic Phenenomena, Vol. 1, (Academic Press: New York, 1966). p. 97. (FTD-MT-64-514), AD-622 356
5. S.I. Braginskii, "Transport Process in a Plasma", in Reviews of Plasma Physics, Vol. 1, ed. M.A. Leontovich, (Consultants Bureau: New York, 1965), p 205.
6. E.A. McLean, private communication.
7. S.T. Kacenjar, B.H. Ripin, J.A. Stamper, J.Grun, and E.A. McLean, NRL Memo Report #5260, "Magnetic Bubble Formation Produced by an Expanding Laser Plasma," (1984). (AD-A139 188)
8. D.A. Tidman, Phys. Fluids, 18, 1454, "Thermally Generated Magnetic Fields in Laser-Driven Compressions and Explosions," (1975).
9. J.A. Stamper, NRL Memo Report #3872, "A Perspective on Self-Generated Magnetic Fields," (1978). (AD-A061 944)
10. M.J. Keskinen, NRL Memo Report # 5163, "Analytic Models of Magnetic Field Evolution in Laser-Produced Plasma Expansions," (1983). (AD-A 132 181)
11. D. Shvartz, J. Delettrez, R.L. McCory, and C.P. Verdon, Physical Review Letters, 47, 247, "Self-Consistent Reduction of the Spitzer-Harm Electron Thermal Heat Flux in Steep Temperature Gradients in Laser-Produced Plasmas,"(1981).
12. R. Courant and K.O. Friedricks, Supersonic Flow and Shock Waves, (Interscience; New York 1977), p. 204.
13. A Solinger, S. Rappaport, and J. Buff, Ap. J., 201, 381, "Isothermal Blast Wave Model of Supernova Remnants," (1975).

14. L.L. Cowie, Ap. J., 215, 226, "The Early Evolution of Supernova Remnants in a Homogeneous Medium: The Effects of Electron Thermal Conduction," (1977).

15. S. Brecht, Early-Time High-Altitude News letter, Issue 3 (1983).

16. J. Stamper, private communication.

DISTRIBUTION LIST

DEPARTMENT OF DEFENSE

ASSISTANT SECRETARY OF DEFENSE
COMM, CMD, CONT 7 INTELL
WASHINGTON, D.C. 20301

DIRECTOR
COMMAND CONTROL TECHNICAL CENTER
PENTAGON RM BE 685
WASHINGTON, D.C. 20301
01CY ATTN C-650
01CY ATTN C-312 R. MASON

DIRECTOR
DEFENSE ADVANCED RSCH PROJ AGENCY
ARCHITECT BUILDING
1400 WILSON BLVD.
ARLINGTON, VA. 22209
01CY ATTN NUCLEAR
MONITORING RESEARCH
01CY ATTN STRATEGIC TECH OFFICE

DEFENSE COMMUNICATION ENGINEER CENTER
1860 WIEHLE AVENUE
RESTON, VA. 22090
01CY ATTN CODE R410
01CY ATTN CODE R812

DEFENSE TECHNICAL INFORMATION CENTER
CAMERON STATION
ALEXANDRIA, VA. 22314
02CY

DIRECTOR
DEFENSE NUCLEAR AGENCY
WASHINGTON, D.C. 20305
01CY ATTN STVL
04CY ATTN TITL
01CY ATTN DDST
03CY ATTN RAAE

COMMANDER
FIELD COMMAND
DEFENSE NUCLEAR AGENCY
KIRTLAND, AFB, NM 87115
01CY ATTN FCPR

DEFENSE NUCLEAR AGENCY
SAO/DNA
BUILDING 20676
KIRTLAND AFB, NM 87115
01CY D.C. THORNBURG

DIRECTOR
INTERSERVICE NUCLEAR WEAPONS SCHOOL
KIRTLAND AFB, NM 87115
01CY ATTN DOCUMENT CONTROL

JOINT CHIEFS OF STAFF
WASHINGTON, D.C. 20301
01CY ATTN J-3 WWMCCS EVALUATION
OFFICE

DIRECTOR
JOINT STRAT TGT PLANNING STAFF
OFFUTT AFB
OMAHA, NB 68113
01CY ATTN JLTW-2
01CY ATTN JPST G. GOETZ

CHIEF
LIVERMORE DIVISION FLD COMMAND DNA
DEPARTMENT OF DEFENSE
LAWRENCE LIVERMORE LABORATORY
P.O. BOX 808
LIVERMORE, CA 94550
01CY ATTN FCPRL

COMMANDANT
NATO SCHOOL (SHAPE)
APO NEW YORK 09172
01CY ATTN U.S. DOCUMENTS OFFICER

UNDER SECY OF DEF FOR RSCH & ENGRG
DEPARTMENT OF DEFENSE
WASHINGTON, D.C. 20301
01CY ATTN STRATEGIC & SPACE
SYSTEMS (OS)

WWMCCS SYSTEM ENGINEERING ORG
WASHINGTON, D.C. 20305
01CY ATTN R. CRAWFORD

COMMANDER/DIRECTOR
ATMOSPHERIC SCIENCES LABORATORY
U.S. ARMY ELECTRONICS COMMAND
WHITE SANDS MISSILE RANGE, NM 88002
01CY ATTN DELAS-EO, F. NILES

DIRECTOR
BMD ADVANCED TECH CTR
HUNTSVILLE OFFICE
P.O. BOX 1500
HUNTSVILLE, AL 35807
01CY ATTN ATC-T MELVIN T. CAPPS
01CY ATTN ATC-O W. DAVIES
01CY ATTN ATC-R DON RUSS

PROGRAM MANAGER
BMD PROGRAM OFFICE
5001 EISENHOWER AVENUE
ALEXANDRIA, VA 22333
01CY ATTN DACS-BMT J. SHEA

CHIEF C-E- SERVICES DIVISION
U.S. ARMY COMMUNICATIONS CMD
PENTAGON RM 1B269
WASHINGTON, D.C. 20310
01CY ATTN C- E-SERVICES DIVISION

COMMANDER
FRADCOM TECHNICAL SUPPORT ACTIVITY
DEPARTMENT OF THE ARMY
FORT MONMOUTH, N.J. 07703
01CY ATTN DRSEL-NL-RD H. BENNET
01CY ATTN DRSEL-PL-ENV H. BOMKE
01CY ATTN J.E. QUIGLEY

COMMANDER
U.S. ARMY COMM-ELEC ENGRG INSTAL AGY
FT. HUACHUCA, AZ 85613
01CY ATTN CCC-EMEO GEORGE LANE

COMMANDER
U.S. ARMY FOREIGN SCIENCE & TECH CTR
220 7TH STREET, NE
CHARLOTTESVILLE, VA 22901
01CY ATTN DRXST-SD

COMMANDER
U.S. ARMY MATERIAL DEV & READINESS CMD
5001 EISENHOWER AVENUE
ALEXANDRIA, VA 22333
01CY ATTN DRCLDC J.A. BENDER

COMMANDER
U.S. ARMY NUCLEAR AND CHEMICAL AGENCY
7500 BACKLICK ROAD
BLDG 2073
SPRINGFIELD, VA 22150
01CY ATTN LIBRARY

DIRECTOR
U.S. ARMY BALLISTIC RESEARCH
LABORATORY
ABERDEEN PROVING GROUND, MD 21005
01CY ATTN TECH LIBRARY,
EDWARD BAICY

COMMANDER
U.S. ARMY SATCOM AGENCY
FT. MONMOUTH, NJ 07703
01CY ATTN DOCUMENT CONTROL

COMMANDER
U.S. ARMY MISSILE INTELLIGENCE AGENCY
REDSTONE ARSENAL, AL 35809
01CY ATTN JIM GAMBLE

DIRECTOR
U.S. ARMY TRADOC SYSTEMS ANALYSIS
ACTIVITY
WHITE SANDS MISSILE RANGE, NM 88002
01CY ATTN ATAA-SA
01CY ATTN TCC/F. PAYAN JR.
01CY ATTN ATTA-TAC LTC J. HESSE

COMMANDER
NAVAL ELECTRONIC SYSTEMS COMMAND
WASHINGTON, D.C. 20360
01CY ATTN NAVALEX 034 T. HUGHES
01CY ATTN PME 117
01CY ATTN PME 117-T
01CY ATTN CODE 5011

COMMANDING OFFICER
NAVAL INTELLIGENCE SUPPORT CTR
4301 SUITLAND ROAD, BLDG. 5
WASHINGTON, D.C. 20390
01CY ATTN MR. DUBBIN STIC 12
01CY ATTN NISC-50
01CY ATTN CODE 5404 J. GALET

COMMANDER
NAVAL OCCEAN SYSTEMS CENTER
SAN DIEGO, CA 92152
01CY ATTN J. FERGUSON

NAVAL RESEARCH LABORATORY
WASHINGTON, D.C. 20375
01CY ATTN CODE 4700 S. L. Ossakow
26 CYS IF UNCLASS. 1 CY
IF CLASS)
01CY ATTN CODE 4701 I Vitkovitsky
01CY ATTN CODE 4780 J. Huba (100
CYS IF UNCLASS, 1 CY IF CLASS)
01CY ATTN CODE 7500
01CY ATTN CODE 7550
01CY ATTN CODE 7580
01CY ATTN CODE 7551
01CY ATTN CODE 7555
01CY ATTN CODE 4730 E. MCLEAN
01CY ATTN CODE 4108
01CY ATTN CODE 4730 B. RIPIN
20CY ATTN CODE 2628

COMMANDER
NAVAL SEA SYSTEMS COMMAND
WASHINGTON, D.C. 20362
01CY ATTN CAPT R. PITKIN

COMMANDER
NAVAL SPACE SURVEILLANCE SYSTEM
DAHLGREN, VA 22448
01CY ATTN CAPT J.H. BURTON

OFFICER-IN-CHARGE
NAVAL SURFACE WEAPONS CENTER
WHITE OAK, SILVER SPRING, MD 20910
01CY ATTN CODE F31

DIRECTOR
STRATEGIC SYSTEMS PROJECT OFFICE
DEPARTMENT OF THE NAVY
WASHINGTON, D.C. 20376
01CY ATTN NSP-2141
01CY ATTN NSSP-2722 FRED WIMBERLY

COMMANDER
NAVAL SURFACE WEAPONS CENTER
DAHLGREN LABORATORY
DAHLGREN, VA 22448
01CY ATTN CODE DF-14 R. BUTLER

OFFICER OF NAVAL RESEARCH
ARLINGTON, VA 22217
01CY ATTN CODE 465
01CY ATTN CODE 461
01CY ATTN CODE 402
01CY ATTN CODE 420
01CY ATTN CODE 421

COMMANDER
AEROSPACE DEFENSE COMMAND/DC
DEPARTMENT OF THE AIR FORCE
ENT AFB, CO 80912
01CY ATTN DC MR. LONG

COMMANDER
AEROSPACE DEFENSE COMMAND/XPD
DEPARTMENT OF THE AIR FORCE
ENT AFB, CO 80912
01CY ATTN XPDQQ
01CY ATTN XP

AIR FORCE GEOPHYSICS LABORATORY
HANSCOM AFB, MA 01731
01CY ATTN OPR HAROLD GARDNER
01CY ATTN LKB
KENNETH S.W. CHAMPION
01CY ATTN OPR ALVA T. STAIR
01CY ATTN PHD JURGEN BUCHAU
01CY ATTN PHD JOHN P. MULLEN

AF WEAPONS LABORATORY
KIRTLAND AFT, NM 87117
01CY ATTN SUL
01CY ATTN CA ARTHUR H. GUENTHER
01CY ATTN NTYCE 1LT. G. KRAJEI

AFTAC
PATRICK AFB, FL 32925
01CY ATTN TF/MAJ WILEY
01CY ATTN TN

AIR FORCE AVIONICS LABORATORY
WRIGHT-PATTERSON AFB, OH 45433
01CY ATTN AAD WADE HUNT
01CY ATTN AAD ALLEN JOHNSON

DEPUTY CHIEF OF STAFF
RESEARCH, DEVELOPMENT, & ACQ
DEPARTMENT OF THE AIR FORCE
WASHINGTON, D.C. 20330
01CY ATTN AFRDQ

HEADQUARTERS
ELECTRONIC SYSTEMS DIVISION
DEPARTMENT OF THE AIR FORCE
HANSCOM AFB, MA 01731
01CY ATTN J. DEAS

HEADQUARTERS
ELECTRONIC SYSTEMS DIVISION/YSEA
DEPARTMENT OF THE AIR FORCE
HANSCOM AFB, MA 01732
01CY ATTN YSEA

HEADQUARTERS
ELECTRONIC SYSTEMS DIVISION/DC
DEPARTMENT OF THE AIR FORCE
HANSCOM AFB, MA 01731
01CY ATTN DCKC MAJ J.C. CLARK

COMMANDER
FOREIGN TECHNOLOGY DIVISION, AFSC
WRIGHT-PATTERSON AFB, OH 45433
01CY ATTN NICD LIBRARY
01CY ATTN ETDP B. BALLARD

COMMANDER
ROME AIR DEVELOPMENT CENTER, AFSC
GRIFFISS AFB, NY 13441
01CY ATTN DOC LIBRARY/TSLD
01CY ATTN OCSE V. COYNE

SAMSO/SZ
POST OFFICE BOX 92960
WORLDWAY POSTAL CENTER
LOS ANGELES, CA 90009
(SPACE DEFENSE SYSTEMS)
01CY ATTN SZJ

STRATEGIC AIR COMMAND/XPFS
OFFUTT AFB, NB 68113
01CY ATTN ADWATE MAJ BRUCE BAUER
01CY ATTN NRT
01CY ATTN DOK CHIEF SCIENTIST

SAMSO/SK
P.O. BOX 92960
WORLDWAY POSTAL CENTER
LOS ANGELES, CA 90009
01CY ATTN SKA (SPACE COMM SYSTEMS)
M. CLAVIN

SAMSO/MN
NORTON AFB, CA 92409
(MINUTEMAN)
01CY ATTN MNNL

COMMANDER
ROME AIR DEVELOPMENT CENTER, AFSC
HANSCOM AFB, MA 01731
01CY ATTN EEP A. LORENTZEN

DEPARTMENT OF ENERGY
LIBRARY ROOM G-042
WASHINGTON, D.C. 20545
01CY ATTN DOC CON FOR A. LABOWITZ

DEPARTMENT OF ENERGY
ALBUQUERQUE OPERATIONS OFFICE
P.O. BOX 5400
ALBUQUERQUE, NM 87115
01CY ATTN DOC CON FOR D. SHERWOOD

EG&G, INC.
LOS ALAMOS DIVISION
P.O. BOX 809
LOS ALAMOS, NM 85544
01CY ATTN DOC CON FOR J. BREEDLOVE

UNIVERSITY OF CALIFORNIA
LAWRENCE LIVERMORE LABORATORY
P.O. BOX 808
LIVERMORE, CA 94550
01CY ATTN DOC CON FOR TECH INFO
DEPT
01CY ATTN DOC CON FOR L-389 R. OTT
01CY ATTN DOC CON FOR L-31 R. HAGER

LOS ALAMOS NATIONAL LABORATORY
P.O. BOX 1663
LOS ALAMOS, NM 87545
01CY ATTN DOC CON FOR J. WOLCOTT
01CY ATTN DOC CON FOR R.F. TASCHEK
01CY ATTN DOC CON FOR E. JONES
01CY ATTN DOC CON FOR J. MALIK
01CY ATTN DOC CON FOR R. JEFFRIES
01CY ATTN DOC CON FOR J. ZINN
01CY ATTN DOC CON FOR P. KEATON
01CY ATTN DOC CON FOR D. WESTERVELT
01CY ATTN D. SAPPENFIELD

SANDIA LABORATORIES
P.O. BOX 5800
ALBUQUERQUE, NM 87115
01CY ATTN DOC CON FOR W. BROWN
01CY ATTN DOC CON FOR A.
THORNBROUGH
01CY ATTN DOC CON FOR T. WRIGHT
01CY ATTN DOC CON FOR D. DAHLGREN
01CY ATTN DOC CON FOR 3141
01CY ATTN DOC CON FOR SPACE PROJECT
DIV

SANDIA LABORATORIES
LIVERMORE LABORATORY
P.O. BOX 969
LIVERMORE, CA 94550
01CY ATTN DOC CON FOR B. MURPHEY
01CY ATTN DOC CON FOR T. COOK

OFFICE OF MILITARY APPLICATION
DEPARTMENT OF ENERGY
WASHINGTON, D.C. 20545
01CY ATTN DOC CON DR. YO SONG

OTHER GOVERNMENT

INSTITUTE FOR TELECOM SCIENCES
NATIONAL TELECOMMUNICATIONS & INFO ADMIN
BOULDER, CO 80303
01CY ATTN A. JEAN (UNCLASS ONLY)
01CY ATTN W. UTLAUT
01CY ATTN D. CROMBIE
01CY ATTN L. BERRY

NATIONAL OCEANIC & ATMOSPHERIC ADMIN
ENVIRONMENTAL RESEARCH LABORATORIES
DEPARTMENT OF COMMERCE
BOULDER, CO 80302
01CY ATTN R. GRUBB
01CY ATTN AERONOMY LAB G. REID

DEPARTMENT OF DEFENSE CONTRACTORS

AEROSPACE CORPORATION
P.O. BOX 92957
LOS ANGELES, CA 90009
01CY ATTN I. GARFUNKEL
01CY ATTN T. SALMI
01CY ATTN V. JOSEPHSON
01CY ATTN S. BOWER
01CY ATTN D. OLSEN

ANALYTICAL SYSTEMS ENGINEERING CORP
5 OLD CONCORD ROAD
BURLINGTON, MA 01803
01CY ATTN RADIO SCIENCES

AUSTIN RESEARCH ASSOC., INC.
1901 RUTLAND DRIVE
AUSTIN, TX 78758
01CY ATTN L. SLOAN
01CY ATTN R. THOMPSON

BERKELEY RESEARCH ASSOCIATES, INC.
P.O. BOX 983
BERKELEY, CA 94701
01CY ATTN J. WORKMAN
01CY ATTN C. PRETTIE
01CY ATTN S. BRECHT

BOEING COMPANY, THE
P.O. BOX 3707
SEATTLE, WA 98124
01CY ATTN G. KEISTER
01CY ATTN D. MURRAY
01CY ATTN G. HALL
01CY ATTN J. KENNEY

CHARLES STARK DRAPER LABORATORY, INC.
555 TECHNOLOGY SQUARE
CAMBRIDGE, MA 02139
01CY ATTN D.B. COX
01CY ATTN J.P. GILMORE

COMSAT LABORATORIES
LINTHICUM ROAD
CLARKSBURG, MD 20734
01CY ATTN G. HYDE

CORNELL UNIVERSITY
DEPARTMENT OF ELECTRICAL ENGINEERING
ITHACA, NY 14850
01CY ATTN D.T. FARLEY, JR.

ELECTROSPACE SYSTEMS, INC.
BOX 1359
RICHARDSON, TX 75080
01CY ATTN H. LOGSTON
01CY ATTN SECURITY (PAUL PHILLIPS)

EOS TECHNOLOGIES, INC.
606 Wilshire Blvd.
Santa Monica, Calif 90401
01CY ATTN C.B. GABBARD
01CY ATTN R. LELEVIER

ESL, INC.
495 JAVA DRIVE
SUNNYVALE, CA 94086
01CY ATTN J. ROBERTS
01CY ATTN JAMES MARSHALL

GENERAL ELECTRIC COMPANY
SPACE DIVISION
VALLEY FORGE SPACE CENTER
GODDARD BLVD KING OF PRUSSIA
P.O. BOX 8555
PHILADELPHIA, PA 19101
01CY ATTN M.H. BORTNER
SPACE SCI LAB

GENERAL ELECTRIC COMPANY
P.O. BOX 1122
SYRACUSE, NY 13201
01CY ATTN F. REIBERT

GENERAL ELECTRIC TECH SERVICES
CO., INC.
HMES
COURT STREET
SYRACUSE, NY 13201
01CY ATTN G. MILLMAN

GEOPHYSICAL INSTITUTE
UNIVERSITY OF ALASKA
FAIRBANKS, AK 99701
(ALL CLASS ATTN: SECURITY OFFICER)
01CY ATTN T.N. DAVIS (UNCLASS ONLY)
01CY ATTN TECHNICAL LIBRARY
01CY ATTN NEAL BROWN (UNCLASS ONLY)

GTE SYLVANIA, INC.
ELECTRONICS SYSTEMS GRP-EASTERN DIV
77 A STREET
NEEDHAM, MA 02194
01CY ATTN DICK STEINHOF

HSS, INC.
2 ALFRED CIRCLE
BEDFORD, MA 01730
01CY ATTN DONALD HANSEN

ILLINOIS, UNIVERSITY OF
107 COBLE HALL
150 DAVENPORT HOUSE
CHAMPAIGN, IL 61820
(ALL CORRES ATTN DAN MCCLELLAND)
01CY ATTN K. YEH

INSTITUTE FOR DEFENSE ANALYSES
1801 NO. BEAUREGARD STREET
ALEXANDRIA, VA 22311
01CY ATTN J.M. AEIN
01CY ATTN ERNEST BAUER
01CY ATTN HANS WOLFARD
01CY ATTN JOEL BENGSTON

INTL TEL & TELEGRAPH CORPORATION
500 WASHINGTON AVENUE
NUTLEY, NJ 07110
01CY ATTN TECHNICAL LIBRARY

JAYCOR
11011 TORREYANA ROAD
P.O. BOX 85154
SAN DIEGO, CA 92138
01CY ATTN J.L. SPERLING

JOHNS HOPKINS UNIVERSITY
APPLIED PHYSICS LABORATORY
JOHNS HOPKINS ROAD
LAUREL, MD 20810
01CY ATTN DOCUMENT LIBRARIAN
01CY ATTN THOMAS POTEMRA
01CY ATTN JOHN DASSOULAS

KAMAN SCIENCES CORP
P.O. BOX 7463
COLORADO SPRINGS, CO 80933
01CY ATTN T. MEAGHER

KAMAN TEMPO-CENTER FOR ADVANCED
STUDIES
816 STATE STREET (P.O DRAWER QQ)
SANTA BARBARA, CA 93102
01CY ATTN DASIAC
01CY ATTN WARREN S. KNAPP
01CY ATTN WILLIAM MCNAMARA
01CY ATTN B. GAMBILL

LINKABIT CORP
10453 ROSELLE
SAN DIEGO, CA 92121
01CY ATTN IRWIN JACOBS

LOCKHEED MISSILES & SPACE CO., INC
P.O. BOX 504
SUNNYVALE, CA 94088
01CY ATTN DEPT 60-12
01CY ATTN D.R. CHURCHILL

LOCKHEED MISSILES & SPACE CO., INC.
3251 HANOVER STREET
PALO ALTO, CA 94304
01CY ATTN MARTIN WALT DEPT 52-12
01CY ATTN W.L. IMHOF DEPT 52-12
01CY ATTN RICHARD G. JOHNSON
DEPT 52-12
01CY ATTN J.B. CLADIS DEPT 52-12

MARTIN MARIETTA CORP
ORLANDO DIVISION
P.O. BOX 5837
ORLANDO, FL 32805
01CY ATTN R. HEFFNER

M.I.T. LINCOLN LABORATORY
P.O. BOX 73
LEXINGTON, MA 02173
01CY ATTN DAVID M. TOWLE
01CY ATTN L. LOUGHLIN
01CY ATTN D. CLARK

MCDONNEL DOUGLAS CORPORATION
5301 BOLSA AVENUE
HUNTINGTON BEACH, CA 92647
01CY ATTN N. HARRIS
01CY ATTN J. MOULE
01CY ATTN GEORGE MROZ
01CY ATTN W. OLSON
01CY ATTN R.W. HALPRIN
01CY ATTN TECHNICAL LIBRARY SERVICES

MISSION RESEARCH CORPORATION
735 STATE STREET
SANTA BARBARA, CA 93101
01CY ATTN P. FISCHER
01CY ATTN W.F. CREVIER
01CY ATTN STEVEN L. GUTSCHE
01CY ATTN R. BOGUSCH
01CY ATTN R. HENDRICK
01CY ATTN RALPH KILB
01CY ATTN DAVE SOWLE
01CY ATTN F. FAJEN
01CY ATTN M. SCHEIBE
01CY ATTN CONRAD L. LONGMIRE
01CY ATTN B. WHITE
01CY ATTN R. STAGAT

MISSION RESEARCH CORP.
1720 RANDOLPH ROAD, S.E.
ALBUQUERQUE, NEW MEXICO 87106
01CY R. STELLINGWERF
01CY M. ALME
01CY L. WRIGHT

MITRE CORPORATION, THE
P.O. BOX 208
BEDFORD, MA 01730
01CY ATTN JOHN MORGANSTERN
01CY ATTN G. HARDING
01CY ATTN C.E. CALLAHAN

MITRE CORP
WESTGATE RESEARCH PARK
1820 DOLLY MADISON BLVD
MCLEAN, VA 22101
01CY ATTN W. HALL
01CY ATTN W. FOSTER

PACIFIC-SIERRA RESEARCH CORP
12340 SANTA MONICA BLVD.
LOS ANGELES, CA 90025
01CY ATTN E.C. FIELD, JR.

PENNSYLVANIA STATE UNIVERSITY
IONOSPHERE RESEARCH LAB
318 ELECTRICAL ENGINEERING EAST
UNIVERSITY PARK, PA 16802
(NO CLASS TO THIS ADDRESS)
01CY ATTN IONOSPHERIC RESEARCH LAB

PHOTOMETRICS, INC.
4 ARROW DRIVE
WOBURN, MA 01801
01CY ATTN IRVING L. KOFSKY

PHYSICAL DYNAMICS, INC.
P.O. BOX 3027
BELLEVUE, WA 98009
01CY ATTN E.J. FREMOUW

PHYSICAL DYNAMICS, INC.
P.O. BOX 10367
OAKLAND, CA 94610
ATTN A. THOMSON

R & D ASSOCIATES
P.O. BOX 9695
MARINA DEL REY, CA 90291
01CY ATTN FORREST GILMORE
01CY ATTN WILLIAM B. WRIGHT, JR.
01CY ATTN WILLIAM J. KARZAS
01CY ATTN H. ORY
01CY ATTN C. MACDONALD
01CY ATTN R. TURCO
01CY ATTN L. DeRAND
01CY ATTN W. TSAI

RAND CORPORATION, THE
1700 MAIN STREET
SANTA MONICA, CA 90406
01CY ATTN CULLEN CRAIN
01CY ATTN ED BEDROZIAN

RAYTHEON CO.
528 BOSTON POST ROAD
SUDBURY, MA 01776
01CY ATTN BARBARA ADAMS

RIVERSIDE RESEARCH INSTITUTE
330 WEST 42nd STREET
NEW YORK, NY 10036
01CY ATTN VINCE TRAPANI

SCIENCE APPLICATIONS, INC.
1150 PROSPECT PLAZA
LA JOLLA, CA 92037
01CY ATTN LEWIS M. LINSON
01CY ATTN DANIEL A. HAMLIN
01CY ATTN E. FRIEMAN
01CY ATTN E.A. STRAKER
01CY ATTN CURTIS A. SMITH

SCIENCE APPLICATIONS, INC
1710 GOODRIDGE DR.
MCLEAN, VA 22102
01CY J. COCKAYNE
01CY E. HYMAN

SRI INTERNATIONAL
333 RAVENSWOOD AVENUE
MENLO PARK, CA 94025
01CY ATTN J. CASPER
01CY ATTN DONALD NEILSON
01CY ATTN ALAN BURNS
01CY ATTN G. SMITH
01CY ATTN R. TSUNODA
01CY ATTN DAVID A. JOHNSON
01CY ATTN WALTER G. CHESNUT
01CY ATTN CHARLES L. RINO
01CY ATTN WALTER JAYE
01CY ATTN J. VICKREY
01CY ATTN RAY L. LEADABRAND
01CY ATTN G. CARPENTER
01CY ATTN G. PRICE
01CY ATTN R. LIVINGSTON
01CY ATTN V. GONZALES
01CY ATTN D. MCDANIEL

TECHNOLOGY INTERNATIONAL CORP
75 WIGGINS AVENUE
BEDFORD, MA 01730
01CY ATTN W.P. BOQUIST

TOYON RESEARCH CO.
P.O. Box 6890
SANTA BARBARA, CA 93111
01CY ATTN JOHN ISE, JR.
01CY ATTN JOEL GARBARINO

TRW DEFENSE & SPACE SYS GROUP
ONE SPACE PARK
REDONDO BEACH, CA 90278
01CY ATTN R. K. PLEBUCH
01CY ATTN S. ALTSCHULER
01CY ATTN D. DEE
01CY ATTN D/ STOCKWELL
SNTF/1575

VISIDYNE
SOUTH BEDFORD STREET
BURLINGTON, MASS 01803
01CY ATTN W. REIDY
01CY ATTN J. CARPENTER
01CY ATTN C. HUMPHREY

UNIVERSITY OF PITTSBURGH
PITTSBURGH, PA 15213
01CY ATTN: N. ZABUSKY

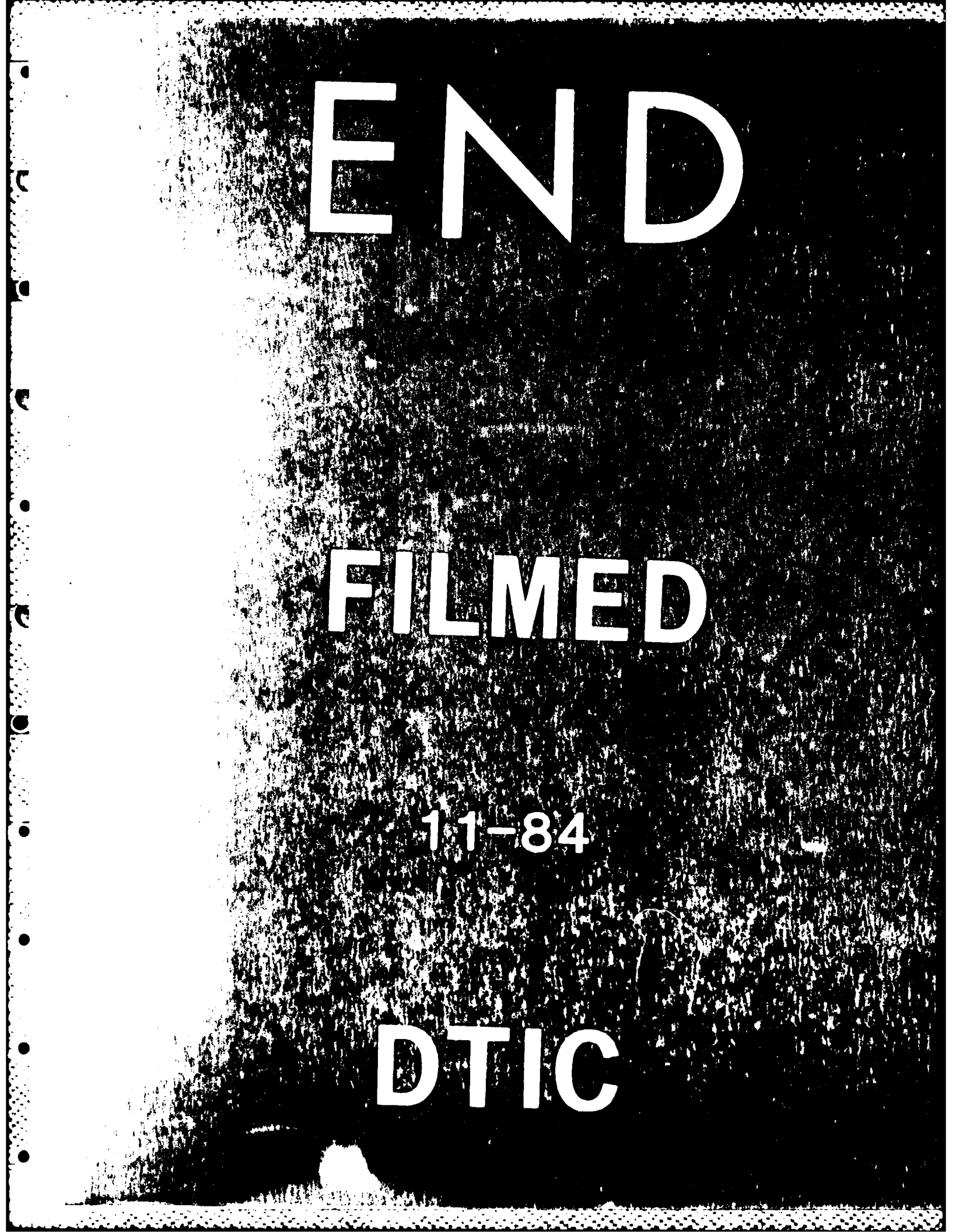
END
FILMED
11-84
DTIC